Supplying Information

Regenerative *In Situ* Formed Bi Nanoparticles on $Bi_2O_2CO_3$ Nanosheets with Bi-Vacancies for Efficient and Stable Photocatalytic CO_2 Reduction to Formate

Donglian Wen[1], Jie Zhao[1], Yang You[1], Liang Huang[1], Haoheng Zhu[1], Chuanghui Zhang[1], Donglei Bu*[1], and Shaoming Huang*[1,2]

[1]School of Materials and Energy, Guangzhou Key Laboratory of Low-Dimensional Materials and Energy Storage Devices, Guangdong University of Technology, Guangzhou 510006, P. R. China

E-mail: budonglei@gdut.edu.cn, smhuang@gdut.edu.cn

[2]School of Chemistry and Materials Science, Hangzhou Institute for Advanced Study University of Chinese Academy of Sciences, Hangzhou, 310024, P. R. China

Materials and Methods

Chemicals

$Bi(NO_3)_3 \cdot 5H_2O$, urea, N-methylpyrrolidine(NMP), Triethanolamine (TEOA), Na_2CO_3, DMSO-d6, KH_2PO_4, and acetonitrile were purchased from Aladdin Chemical Co., Ltd. and used as received.

Methods

Synthesis of $Bi_2O_2CO_3$ Nanosheets (BOC)

The BOC was synthesized using a simple solvent thermal method. First, 0.5 mmol of $Bi_2(NO_3)_3 \cdot 5H_2O$ was dissolved in 30 mL NMP under magnetic stirring. Then 1 g of urea was added to the above solution. The mixture solution was then transferred into a 100 mL Teflon-lined autoclave, and heated at 150 ℃ for 12 h. Solid product was collected by centrifugation with a speed of 10000 rpm, followed by repetitively washing with ethanol and water, and lyophilized overnight.

In situ Reduction of BOC to $Bi^0/Bi_2O_2CO_3$ Nanosheets (BOC-L)

First, 20 mg of the synthetic BOC were dispersed in 10 mL of Triethanolamine (TEOA) solution (TEOA: H_2O=1:9) and mildly sonicated and stirred for 10 min. The dispersion was then transferred to a 100 mL reactor attached to the Labsolar-6A All-glass automatic on-line trace gas analysis system (Perfectlight, Beijing). The system was purged with Ar before illumination. Then the BOC was treated under light (A 300 W Xenon arc lamp, Perfect Light PLS-SXE 300) with various period of time. In the CO_2 photocatalytic process, the reactor containing the in-situ constructed BOC-L were purged with CO_2 to reach atmospheric pressure to reach 90 kPa right after for

photocatalytic performance test. For further characterization, the BOC-L sample were kept in the Ar atmosphere glove box before further analysis.

Regeneration of BOC-L to $Bi_2O_2CO_3$ Nanosheets (BOC-R)

After photocatalysis, the BOC-L samples were washed and centrifugated with ethanol and water, and then dried at 60 ℃. The solids were then dispersed in 0.01 M Na_2CO_3 solution and stirred for 45 mins at 70 ℃, and then washed with water for several times followed by drying at 60 ℃ overnight.

Preparation of $Bi^0/Bi_2O_2CO_3$ without Bi Vacancies (BOC-Bi)

Similar to the method used to prepare BOC-L, except that 19 mg $Bi_2(NO_3)_3 \cdot 5H_2O$ was added in the reactor before illumination here.

Preparation of $Bi_2O_2CO_3$ with Bi Vacancies (BOC-V_{Bi})

20 mg BOC-L powder was dispersed in 50 mL deionized water. The dispersion was rinsed twice with 10 mL 0.1 M acetic acid aqueous solution during suction filtration through a microporous organic filtration membrane. The obtained powder was washed with ethanol and water, then freeze dried.

Ex-situ Preparation of $Bi^0/Bi_2O_2CO_3$

50 mg BOC was dispersed in water firstly. Then, 5mL 0.05M $NaBH_4$ aqueous solution was added in the BOC dispersion. After 10 min stirring at room temperature, the sample was washed with water and ethanol and then lyophilized.

General Methods

Powder X-ray diffraction (PXRD) measurements were collected on a Rigaku Smartlab 9kW X-ray diffractometer using Cu Kα radiation. The BOC-L samples were

taken out from the photocatalytic system in Ar and injected into a sealed centrifuge tube using a syringe to separate the photocatalysts from the liquid. The photocatalysts were kept in a glove box with Ar atmosphere before test. Scanning electron microscope (SEM) characterization was carried out on a Thermo Fisher Apero C scanning electron microscope. Transmission electron microscope (TEM) measurements were carried out on a FEI Talos F200S 200kV scanning/transmission electron microscope. Aberration-corrected scanning transmission electron microscopy (AC-STEM) characterization was carried out on Titan Cubed Themis G2300. The electron paramagnetic resonance (EPR) measurements were performed on a Bruker A300 electron paramagnetic resonance instrument at 298 K with modulation amplitude of 4 Gauss, modulation frequency of 100kHz, sweep width of 3460-3560 mT, number of points of 2000, time constant of 0.01 ms and conversion time 20 ms. The Fourier transform infrared spectra (FT-IR) of the samples were analyzed by infrared spectrometer (Nicolet IS50 Thermo fisher) using KBr disk. The Ultraviolet–visible diffuse reflectance spectra were measured by a UV-vis spectrophotometer (Shimadzu UV-3600), and $BaSO_4$ was used as a reflectance standard material and the scanning range was 200-900 nm. The CO_2 BET adsorption was carried out on a Micromeritics ASAP 2460 at 25℃. Temperature-programmed desorption (TPD) spectroscopy of the samples was performed by using a Micromeritics AutoChem II 2920 with a thermal conductivity detector (TCD).

The VBM of the sample shown in Figure 4B was obtained via the following equation (EQ. S1)

$$VBM_{NHE}=\varphi+E_{VL}-4.44 \qquad \text{EQ. S1}$$

where VBM_{NHE}, E_{VL}, φ are represent the VBM vs NHE (as shown in Figure 4B), the intercept of the tangent with the baseline in the VB-XPS as illustrated in Figure 4B, and the electron work function of the instrument (4.27 eV).

The bandgap energy (Eg) value of the sample could be evaluated using the following equation (EQ. S2)

$$\alpha h\nu = B\,(h\nu - Eg)^2 \qquad \text{EQ. S2}$$

where α is the absorption coefficient, ν is the frequency of the light, h is Planck' s constant, and B is the absorption constant.

The conduction band energy (E_{CB}) photocatalysis could be calculated according to (EQ. S3)

$$E_{CB} = E_{VB} - E_g \qquad \text{EQ. S3}$$

Positron annihilation lifetime spectra (PALS) were done on a fast-fast coincidence lifetime spectrometer (TechnoAP/DPAMS-LCA, Japan) at room temperature. Positron source (^{22}Na, 6.0×10^5 Bq) was sandwiched by two identical tablets (diameter: ∼10.0 mm; thickness: ∼1.5 mm). To get a complete lifetime spectrum, at least 1.8 million counts are needed. Three lifetime components (τ_1, τ_2 and τ_3; I_1, I_2 and I_3) were resolved by using LT 9.0 program.

UPS was conducted using ESCALAB 250Xi (Thermo Fischer) with a He I light source (21.22 eV), and it was calibrated using a gold standard. The working voltage was 12.5 kV, the filament current was 16 mA, and the bias voltage was −10 eV. For the UPS analysis, samples were all pressed to form thin sheets.

Photocatalytic CO_2 Reduction Measurement

The photocatalytic CO_2 reduction measurement was conducted by the Labsolar-6A All-glass automatic on-line trace gas analysis system (Perfectlight, Beijing). In the CO_2 photocatalytic process, the reactor containing the in-situ constructed BOC-L were purged with CO_2 to reach atmospheric pressure to reach 90 kPa. The temperature of the solutions as controlled at 278 ± 0.2 K by a recirculating cooling water system during reaction. Recycling stability test was measured through repeating the above operations including the regeneration treatment before each test.

During reaction, the gas phase products (H_2, O_2, CO, CH_4) were qualitatively analyzed by Agilent 8860 gas chromatograph (TCD or FID detector), using Ar as the carrier gas with a flow rate of 28 mL/min and column temperature of 323.15 K. The detection limit of hydrogen is 1 ppm. The liquid phase products were identified by nuclear magnetic resonance (NMR) (Bruker Avance III HD 600MHz) spectroscopy, and were quantified by reversed phase liquid chromatography (LC) (Acquity UPLC H-Class). Before analysis, a 20 μm filter was used to separate dispersed solids from the liquid. The deuterium reagent of the liquid sample for the ^{1}H NMR spectrum and ^{13}C NMR was DMSO-d6. And the liquid phase of the LC was 0.02 mol/L KH_2PO_4 (pH=3): acetonitrile = 96.5: 3.5.

The apparent quantum efficiency (AQE) of formate produced by photocatalytic CO_2 reduction were tested under low power (3 W) LED (380、420、475、520 and 660 nm). The AQY was calculated by the following formula (EQ. S4)

$$\text{AQE } \% = \frac{number\ of\ reacted\ electrons}{number\ of\ incident\ photons} \times 100$$

$$= \frac{number\ of\ formed\ formate\ molecules\ \times 2}{I \times A \times \lambda} \times 100 \quad \text{EQ. S4}$$

where I and A refers to the optical power density (Wm^{-2}), and the light incident area (m^2), respectively.

Electrochemical Measurement

The electrochemical measurements were measured on a CHI 760E electrochemical station (Shanghai Chenhua, China) in ambient conditions. Generally, 2 mg of photocatalyst were dispersed in 1 mL 1% nafion ethanol solution. A glassy carbon electrode with a photocatalyst deposited served as the working electrode, while a platinum sheet and an Ag/AgCl electrode served as the counter and reference electrode, respectively. The Mott-Schottky measurement were measured in 0.2 M Na_2SO_4 solution. And the typical cyclic voltammetry (CV) curve of BOC nanoosheets were measured in 0.5 M $NaHCO_3$ solution after adjusting the pH to 11. The Linear sweep voltammetry (LSV) was tested in CO_2 saturated 0.5 M $NaHCO_3$ solution after adjusting the pH to 11.

***In-situ* X-ray Photoelectron Spectroscopy (XPS) Measurement**

The *In-situ* X-ray photoelectron spectroscopy (XPS) characterization was carried out on a Thermo Fisher Escalab 250Xi X-ray photoelectron spectrometer, equipped with a 200 mW deuterium light source (190-400 nm). The binding energies obtained in the XPS spectral analysis were corrected for specimen charging by referencing C 1s to 284.8 eV. During the test, the beam spot for the X-ray source (AI target) was 650 μm and the voltage and current were 15 kV and 15 mA, respectively. Before test, the BOC

sample was kept in Ar atmosphere glove box, and then treated with 10^{-5} mbar of Ar in the preparation chamber before transferred to the analysis chamber for XPS measurement. Firstly, a routine XPS test was performed in a dark condition. After finishing the dark condition test, the 200 mW deuterium light source (190-400 nm) was turned on for 90 mins to illuminate the surface of the sample and the XPS test was performed each 30 mins. In order to exclude the influence of X-rays to the illumination, the X-rays should be turned off during the illumination process when the sample not being tested.

***In situ* FTIR Measurement**

In situ FTIR spectra were acquired from Thermo Scientific Nicolet iS50. Firstly, Ar was passed through the dark system for 30 mins in 120°C and the background FT-IR spectra were tested. And then the system was bubbled with pure CO_2 gas (6 mL/min) and H_2O gas for 30 mins to reach the adsorption–desorption equilibrium. After the pre-treatment, the sample was continuously illuminated (near ultraviolet) for 30 mins. The real-time FTIR spectra were collected every 5 mins, and collected once at the moment of light source opening and once at the moment of light source closing.

XRD Refinement

The XRD refinement characterization was carried out on GSASII analysis software, and analyzed with the full spectrum fitting Rietveld method on the basis of the PDF card of tetragonal $Bi_2O_2CO_3$ phase (JCPDS No.84-1752). Before the refinement, the BOC and BOC-L sample were prepared and XRD routine test was measured on a Rigaku Smartlab 9kW X-ray diffractometer using Cu Kα radiation. The

angle range of measurement start from 10° to 90°, and the main peak intensity reached 10000. And the phase formula, cell parameter and R_{WP} were obtained according to the fitting spectrum, which is one of the fitting indexes. Among the refinement result, the lobs (line over background), represents the difference between the intensity of the diffraction peak (or absorption edge) and the background intensity. The lcalc (line calculation) represents the simulated or calculated standard diffraction peak shape, which is a calculation result based on a theoretical model or reference data. The lgkg (line background) represents the shape and intensity of the background, which can be caused by a variety of factors, such as scattering, scattering material, and the background of the diffraction instrument. The lobs-lcalc represents the difference between the actual diffraction peak intensity and the calculated diffraction peak intensity, which can be used to evaluate information such as crystal structure and relative phase content in the sample.

DFT Calculations

The spin-polarized density functional theory (DFT) calculations[1, 2] were carried out in the CP2K/Quickstep package[3] with the hybrid Gaussian and plane wave (GPW) method[4] treat the ion-electron interactions, respectively for structures with distinguished size. The exchange-correlation potential was treated by using a generalized gradient approximation (GGA) with the Perdew-Burke-Ernzerhof (PBE) parametrization.[5] The Gaussian functions consisting of a double-ζ plus polarization (DZVP) basis set in combination of norm conserving Goedecker-Teter-Hutter (GTH) pseudo-potentials was used to describe all elements.[6-8] The Brillouin-zone integration

was sampled with single Gamma point (1 × 1 × 1). The van der Waals correction of Grimme's DFT-D3 model was adopted.[9] The energy cutoff was set to be 600 Ry and the energy convergent standard was 1 x10^{-6} Hartree. The structures were fully relaxed until the maximum force on each atom was less than 4.5 × 10^{-4} Hartree/Bohr. In free energy calculation, the energy convergent standard increased to 1 x10^{-7} Hartree. The Gibbs free energies of the intermediates in CO_2RR were calculated using the following expression:

$$\Delta G = \Delta E + \Delta E_{ZPE} + \Delta H_{0\rightarrow T} - T\Delta S \qquad \text{EQ S5}$$

where ΔE denotes the change in electronic energy obtained from DFT, ΔE_{ZPE}, $\Delta H_{0\rightarrow T}$ and ΔS are the changes of the zero-point energy, the enthalpy and entropy at standard conditions (T = 298 K and at potential *v.s.* NHE).

Supplementary Figures and Tables

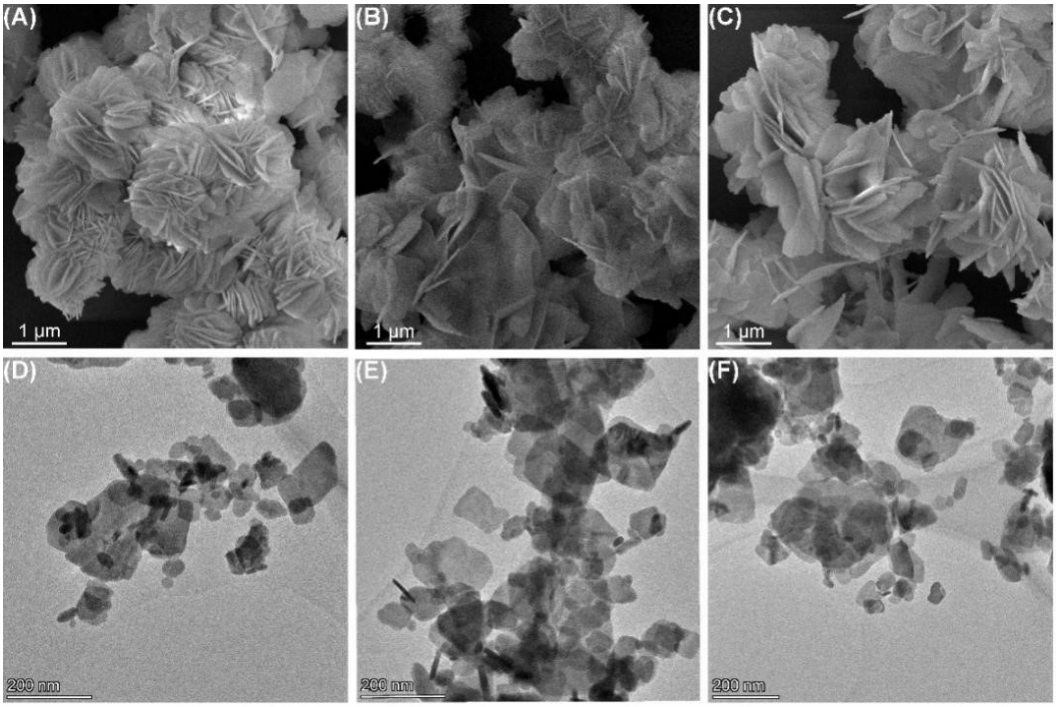

Fig. S1 SEM images of (A) BOC, (B) BOC-L and (C) BOC-R, respectively. TEM images (D) BOC (E) BOC-L and (F) BOC-R, respectively. Scale bar = 1 µm for (A) – (C). Scale bar = 200 nm for (D) – (E).

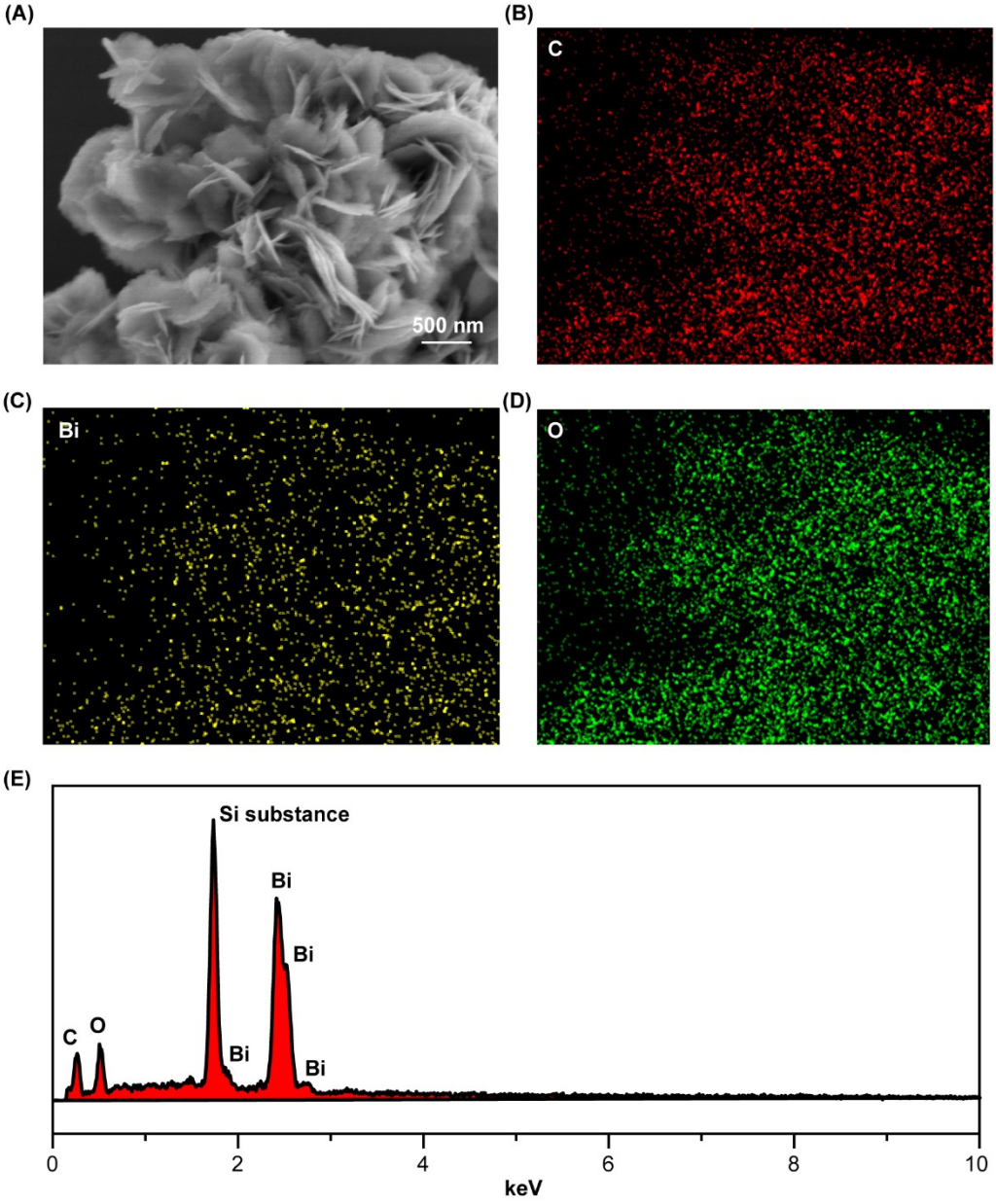

Fig. S2 (A) SEM image, (B)-(D) element mapping images and (E) EDS of BOC.

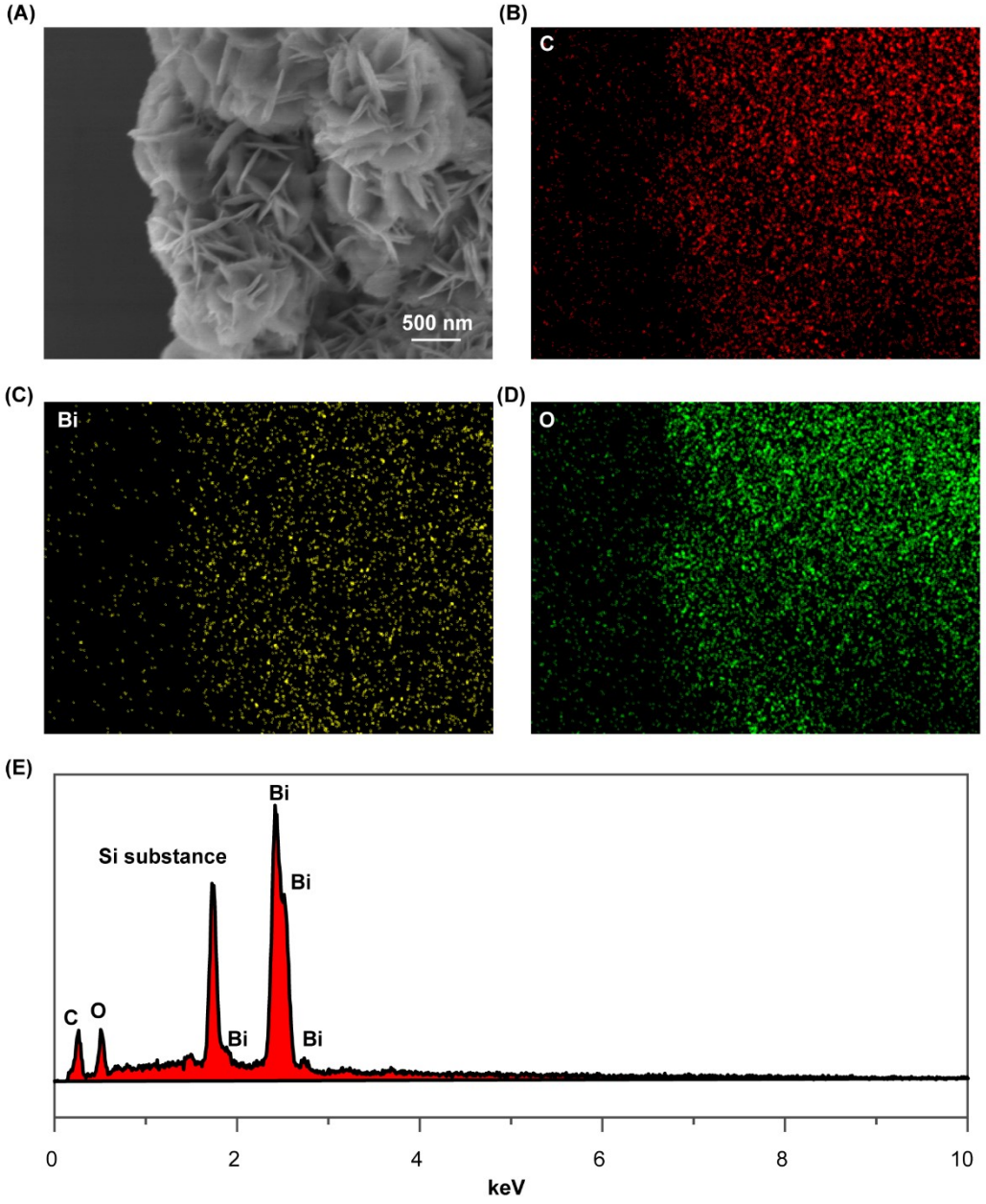

Fig. S3 (A) SEM image, (B)-(D) element mapping images and (E) EDS of BOC-L.

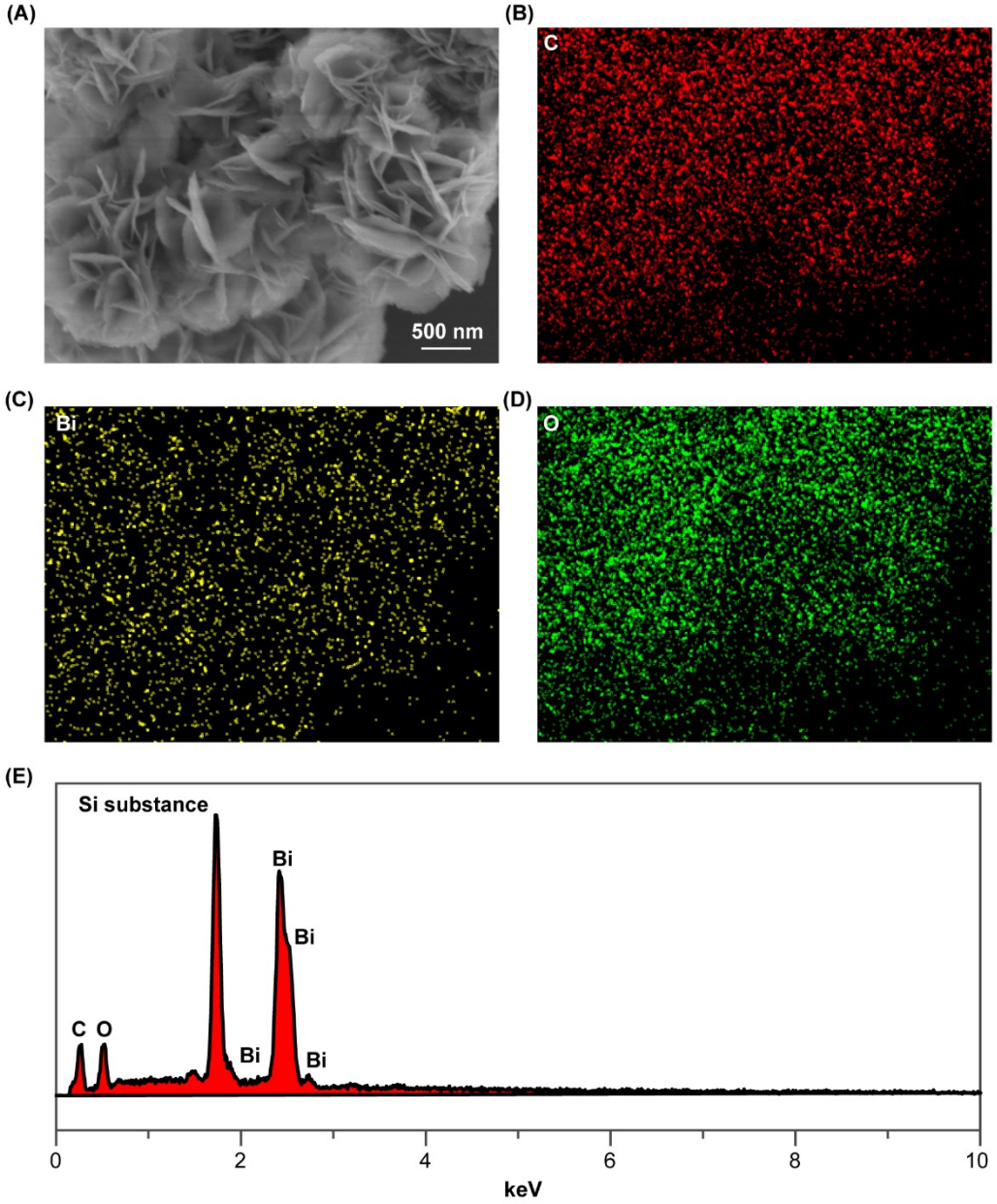

Fig. S4 (A) SEM image, (B)-(D) element mapping images and (E) EDS of BOC-R.

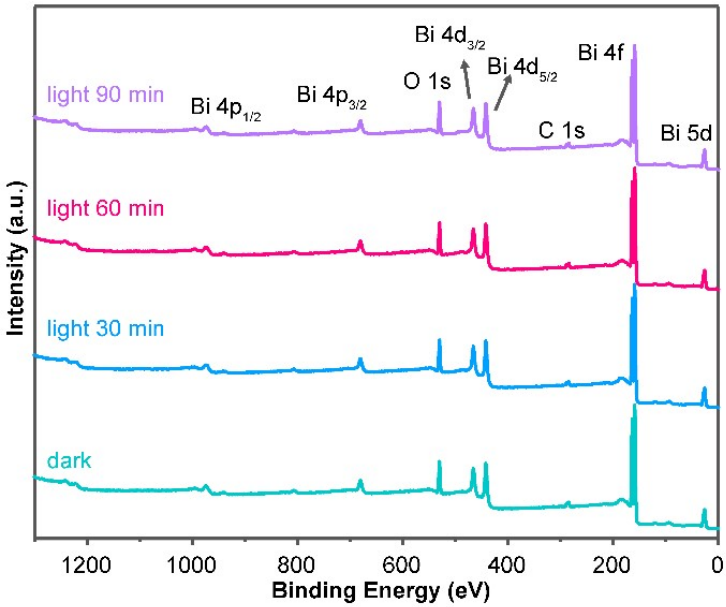

Fig. S5 *In-situ* XPS survey spectra of BOC and BOC-L with different illumination time.

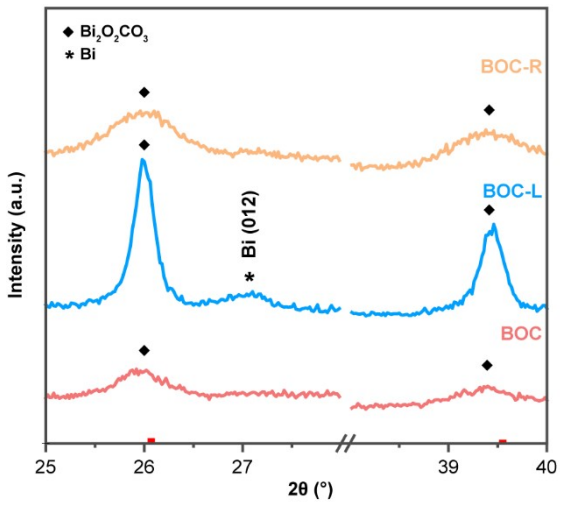

Fig. S6 The enlarged PXRD in the range of 25°to 40° in Fig. 1B.

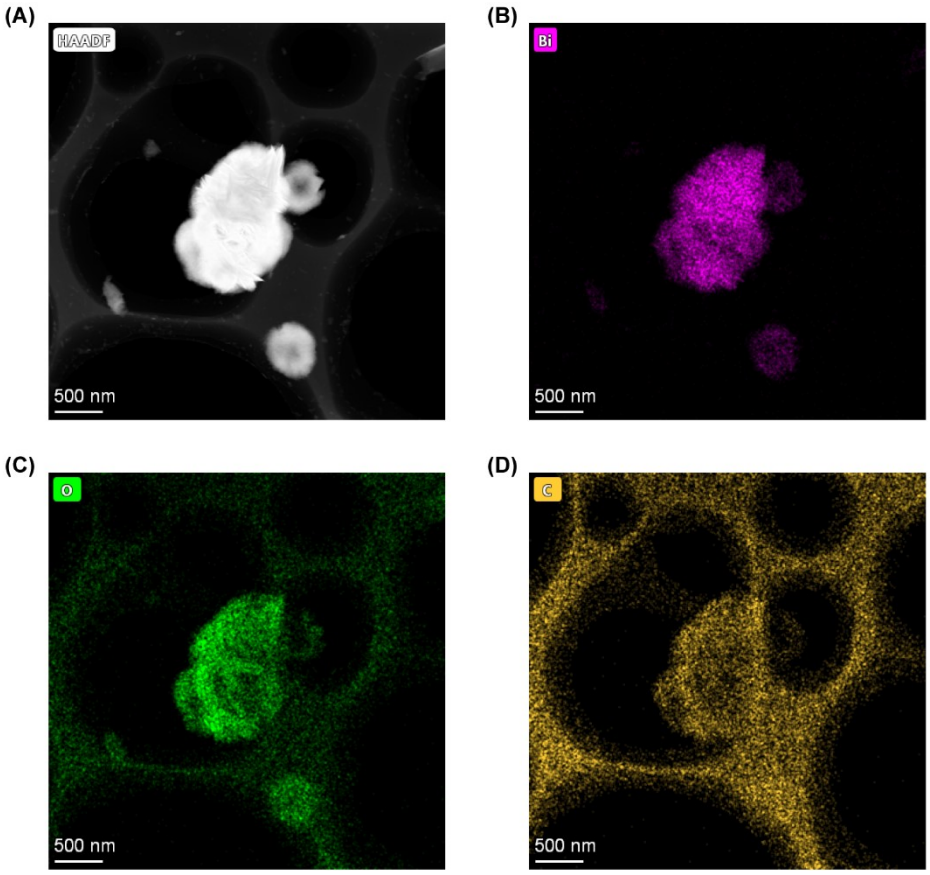

Fig. S7 EDS element mapping images of BOC.

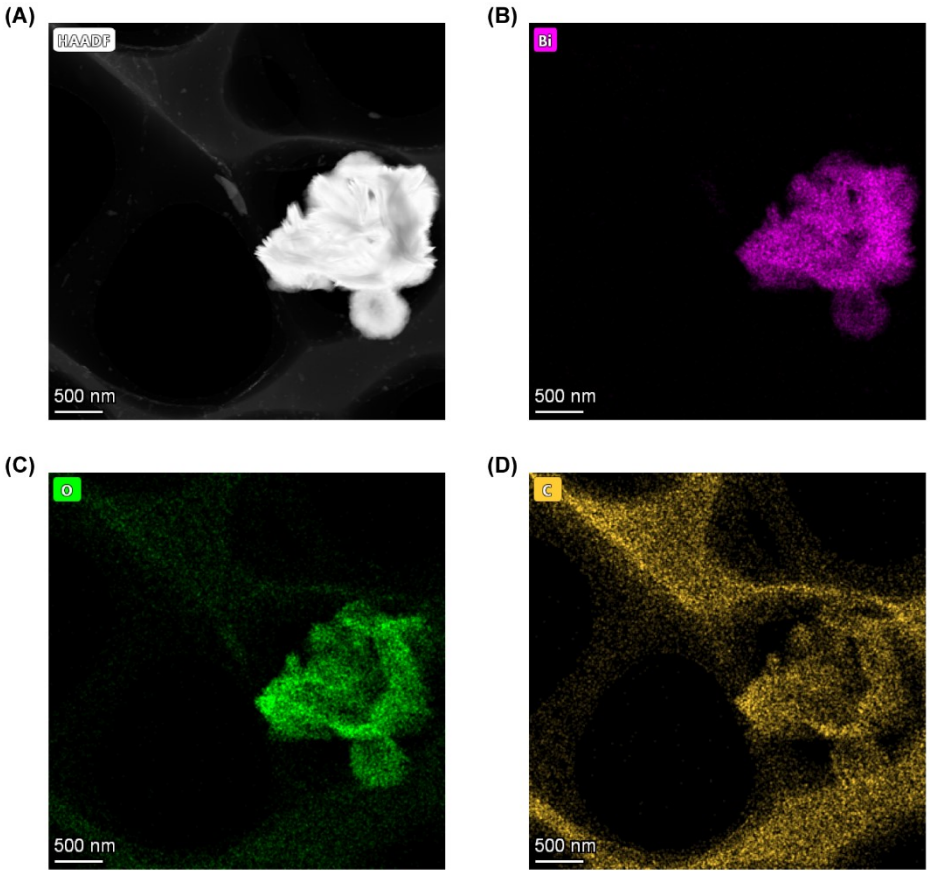

Fig. S8 EDS element mapping images of BOC-L.

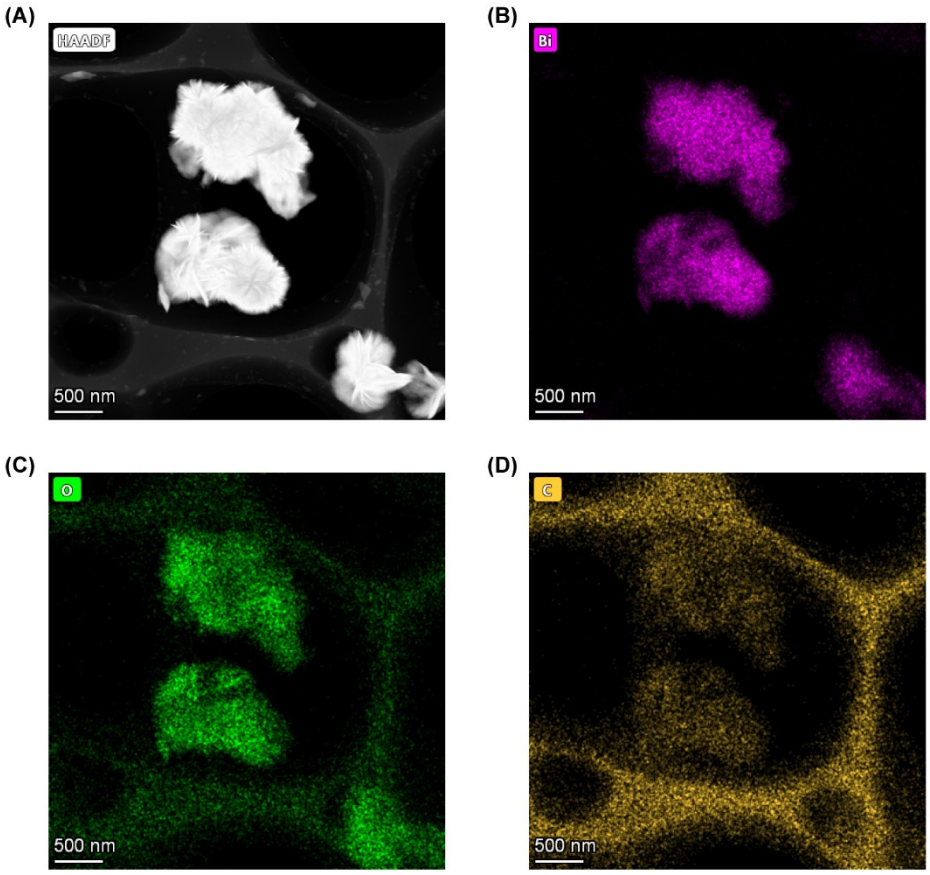

Fig. S9 EDS element mapping images of BOC-R.

Table S1. The FHWM of the highest intensity XRD diffraction peak of $Bi_2O_2CO_3$ of the different samples.

	BOC	BOC-L	BOC-R
2θ (°)	30.2	30.2	30.2
FHWM	0.52122	0.25466	0.57421

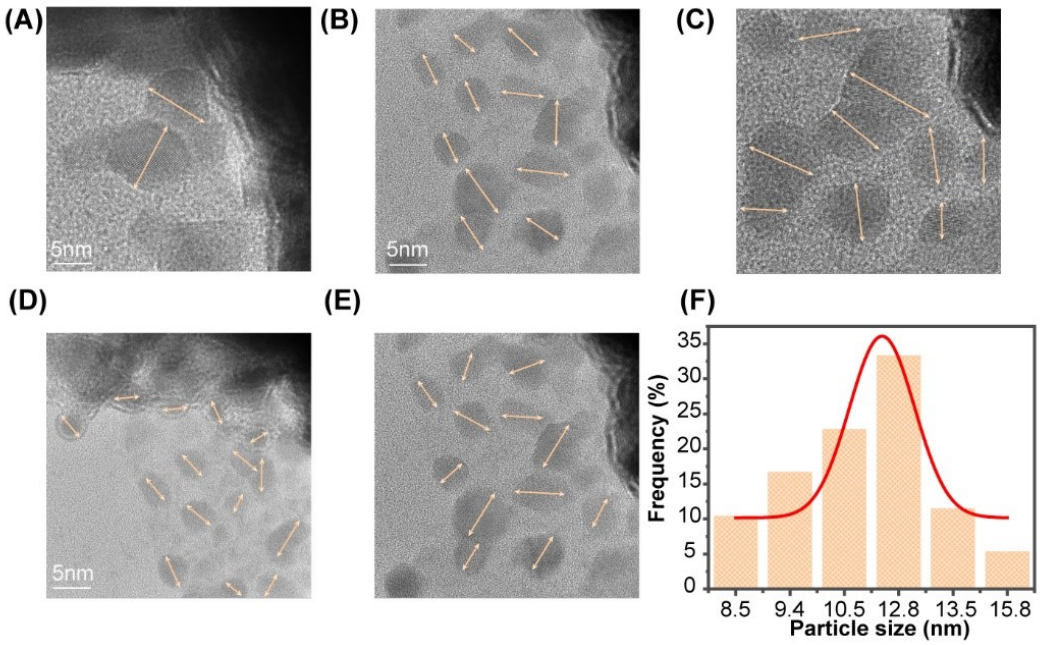

Fig. S10 (A) to (E)The HRTEM images of the BOC-L sample showing the Bi nanoparticles. (F) Size distribution of the Bi nanoparticles of the BOC-L sample measured based on TEM images. The Bi particle size measured based on TEM images (12.6 nm as shown in Fig. S10F) is in good agreement with that estimated according to the Scherrer formula (12.8 nm)

$$D=\frac{K\lambda}{B\cos\theta} \qquad \text{EQ. S5}$$

in which B refers to the full width at half maxima (FWHM) in radians of Bi (012) diffraction peak (0.011122983), K is the Scherrer constant (0.89), θ stands for the Bragg diffraction angle and λ is the X-ray wavelength (in this work, Cu kα with a wavelength of 1.54056 Å was used).

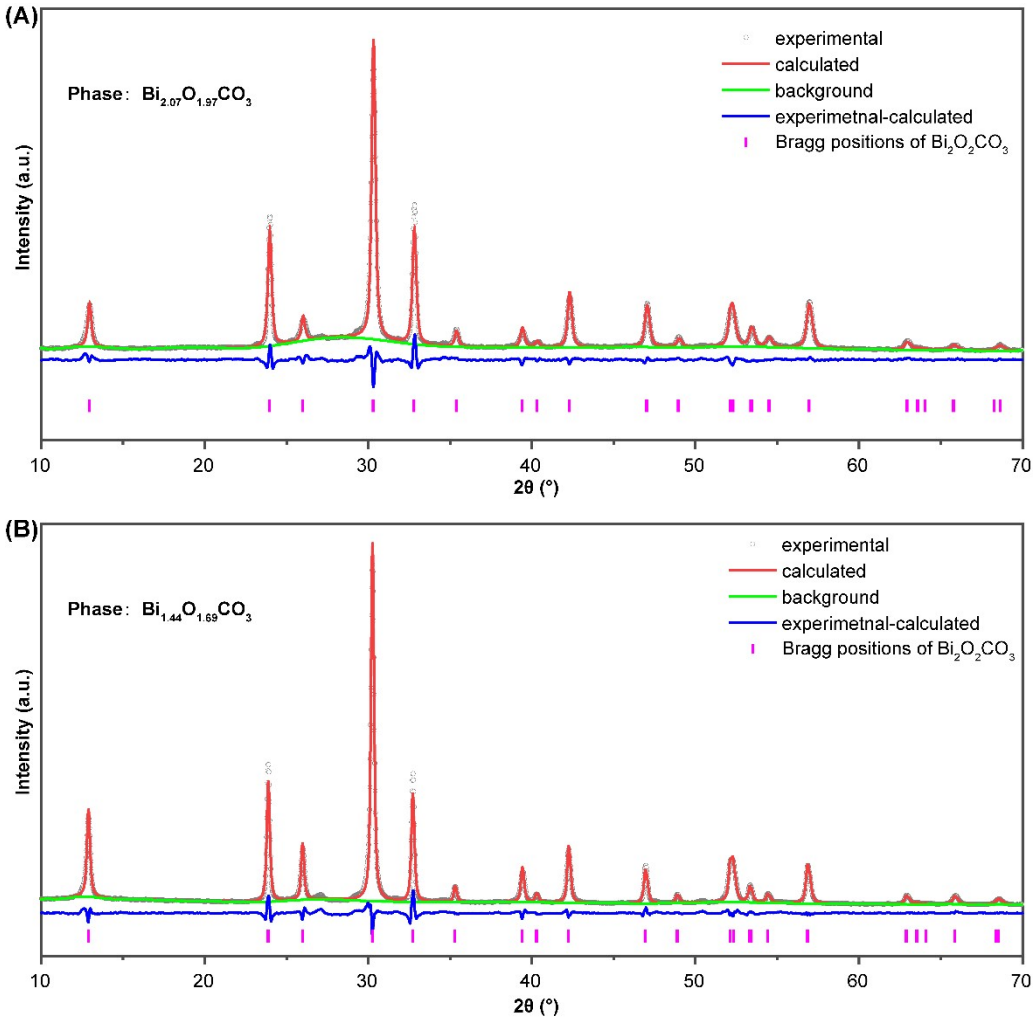

Fig. S11 XRD refinement of (A) BOC and (B) BOC-L.

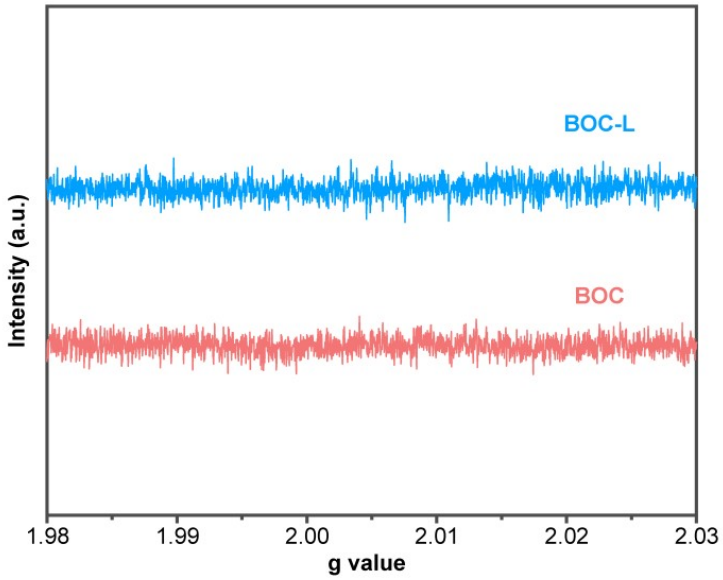

Fig. S12 EPR spectra of BOC and BOC-L.

Table S2. XRD refinement result of BOC and BOC-L.

Parameter \ Sample	BOC	BOC-L
Phase formula	$Bi_{2.07}O_{1.97}CO_3$	$Bi_{1.44}O_{1.69}CO_3$
PDF	JCPDS No.84-1752	JCPDS No.84-1752
Space group	I m m 2	I m m 2
a (Å)	3.87730	3.87670
b (Å)	3.87370	3.87450
c (Å)	13.76590	13.73240
Volume ($Å^3$)	206.756885	206.264410
Fitting index (Rwp)	9.013%	10.744%
Fitting index (GOF)	1.13	1.55

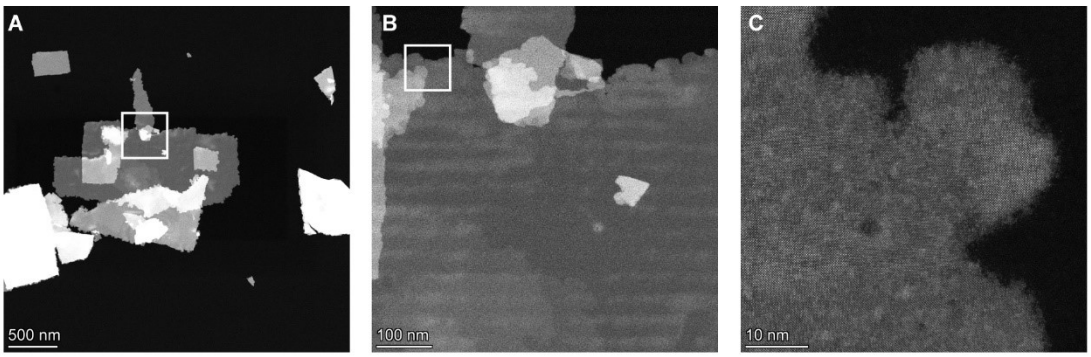

Fig. S13 AC-STEM images of BOC-L at different multiples. The square in (A) and (B) displays the location of (B) and (C) zoomed in (A) and (B) respectively. Scale bar =500 nm for (A) Scale bar = 100 nm for (B) Scale bar = 10 nm for (C)

Table S3. Positron Lifetime Parameters of BOC and BOC-L

Sample	τ_1（ps）	I_1 (%)	τ_2（ps）	I_2 (%)	τ_3（ns）	I_3 (%)
BOC	223.9±1.5	36.34±0.56	359.0±0.7	63.04±0.56	3.38±0.16	0.616±0.017
BOC-L	237.5±4.0	59.6±2.2	381.5±6.2	39.2±2.2	2.462±0.073	1.174±0.056

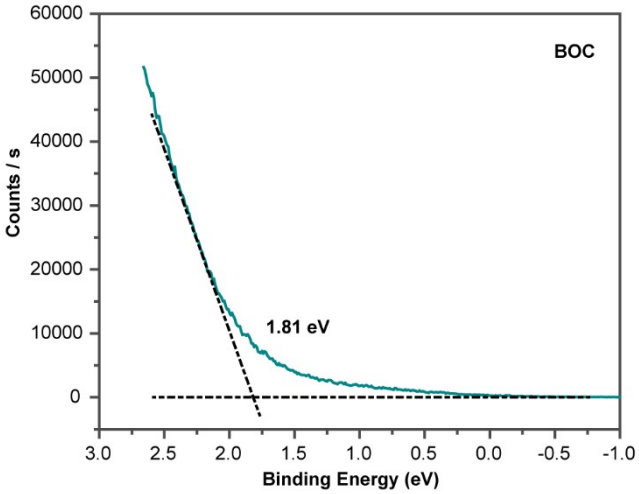

Fig. S14 The VB obtained by UPS spectra of BOC.

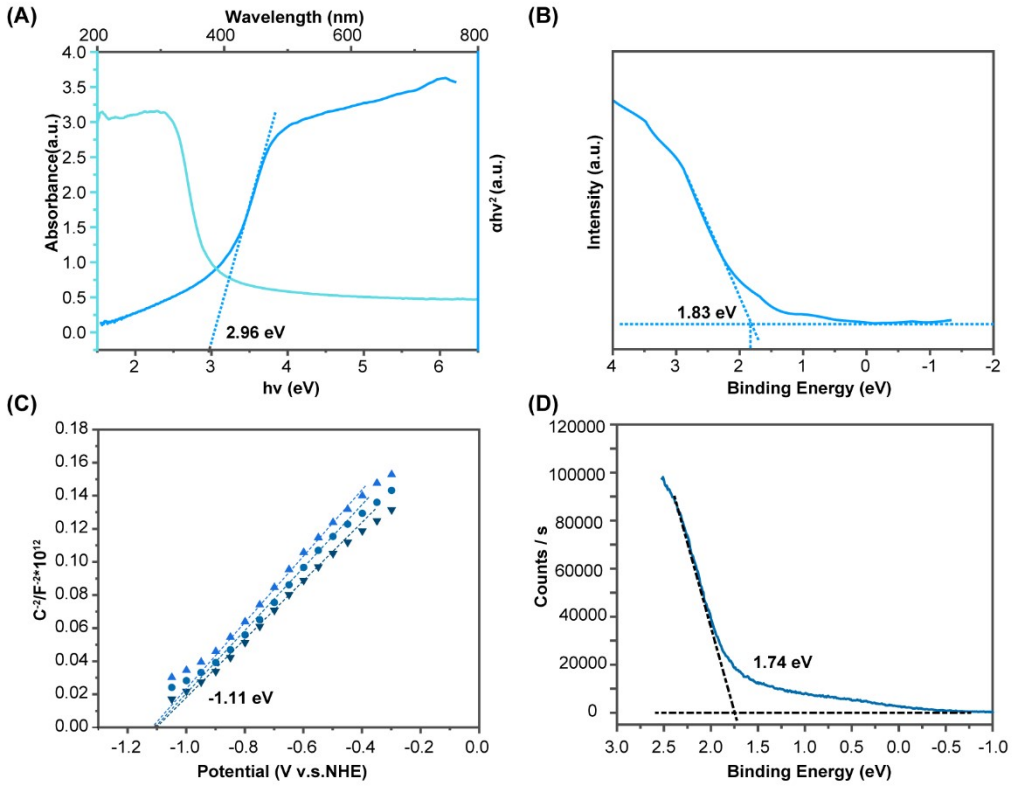

Fig. S15 (A) DRS spectrum (light blue) and plot of transformed Kubelka–Munk function versus photon energy (dark blue), (B) VB-XPS, (C) Mott–Schottky plot, (D) VB obtained by UPS spectra of BOC-L, respectively.

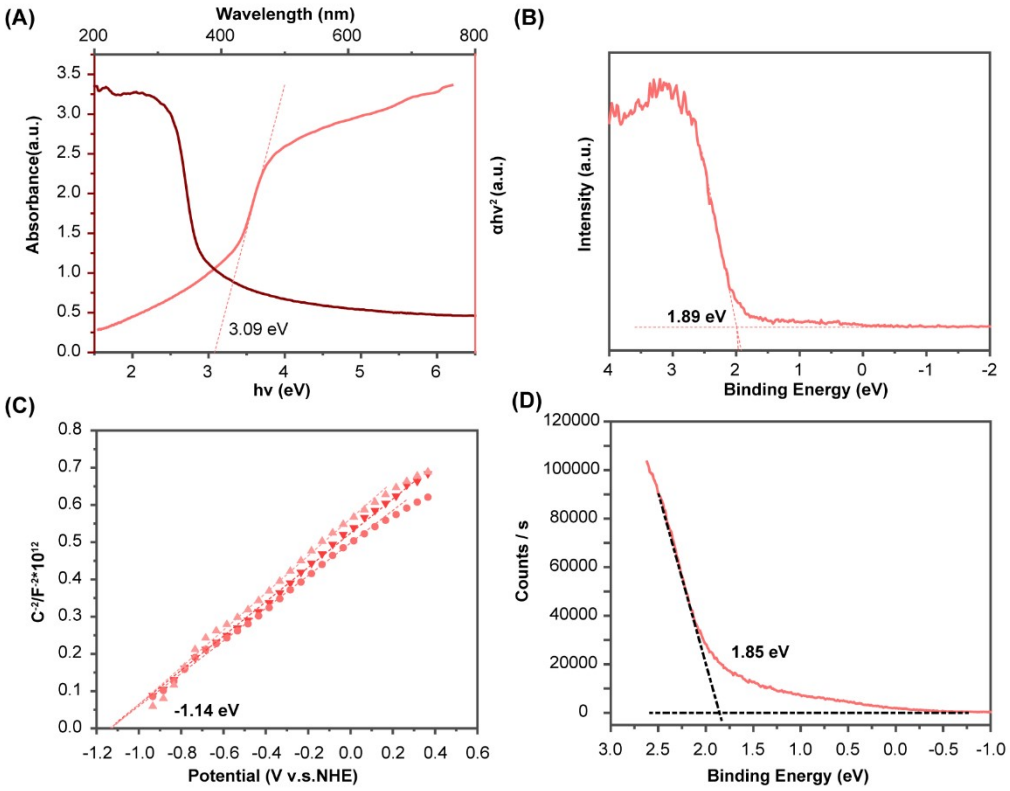

Fig. S16 (A) DRS spectrum (light red) and plot of transformed Kubelka–Munk function versus photon energy (dark red), (B) VB-XPS, (C) Mott–Schottky plot, (D) VB obtained by UPS spectra of BOC-R, respectively.

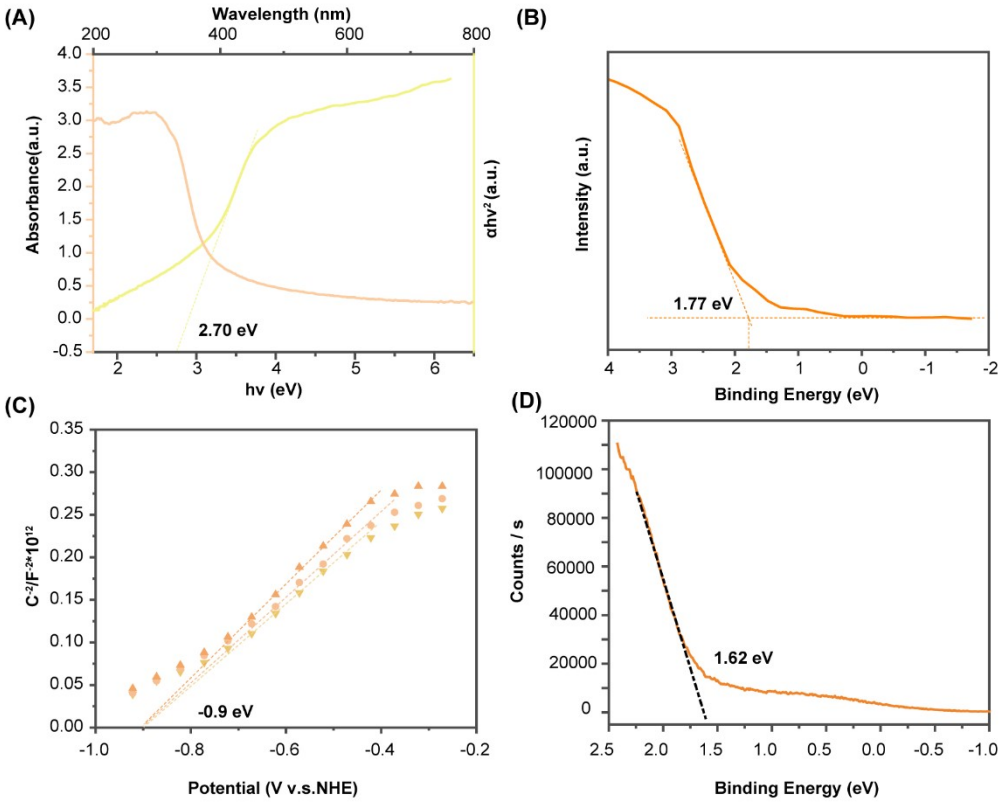

Fig. S17 (A) DRS spectrum (light yellow) and plot of transformed Kubelka–Munk function versus photon energy (orange), (B) VB-XPS, (C) Mott–Schottky plot, (D) VB obtained by UPS spectra of BOC-Bi, respectively.

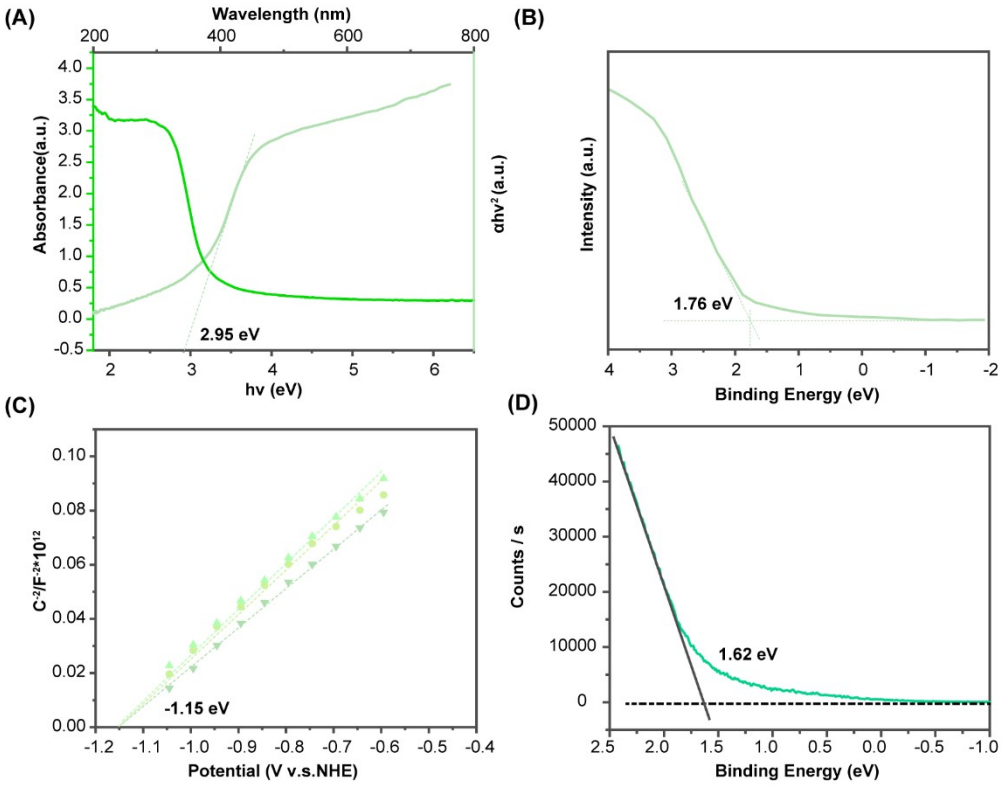

Fig. S18 (A) DRS spectrum (light green) and plot of transformed Kubelka–Munk function versus photon energy (dark green), (B) VB-XPS, (C) Mott–Schottky plot, (D) VB obtained by UPS spectra of BOC-V_{Bi}, respectively.

Table S4. Band Positions Measured via Different Techniques of BOC, BOC-L, BOC-R, BOC-Bi and BOC-V_{Bi}.

Sample	Band Gap (eV)	CBM (V *v.s.* NHE)		VBM (V *v.s.* NHE)	
		DRS + VB-XPS	Mott–Schottky	VB-XPS	UPS
BOC	3.05	-1.34	-1.33	1.71	1.81
BOC-L	2.96	-1.30	-1.31	1.66	1.74
BOC-R	3.09	-1.37	-1.34	1.72	1.85
BOC-Bi	2.70	-1.10	-1.10	1.60	1.62
BOC-V_{Bi}	2.95	-1.36	-1.35	1.59	1.62

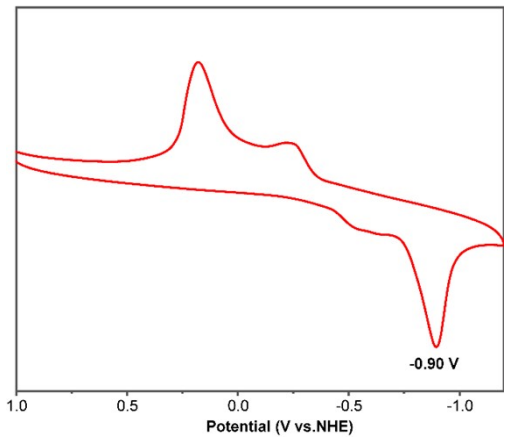

Fig. S19 CV of BOC, the reduction peak shows the potential of Bi^{3+} in BOC reduced to Bi^{0}.

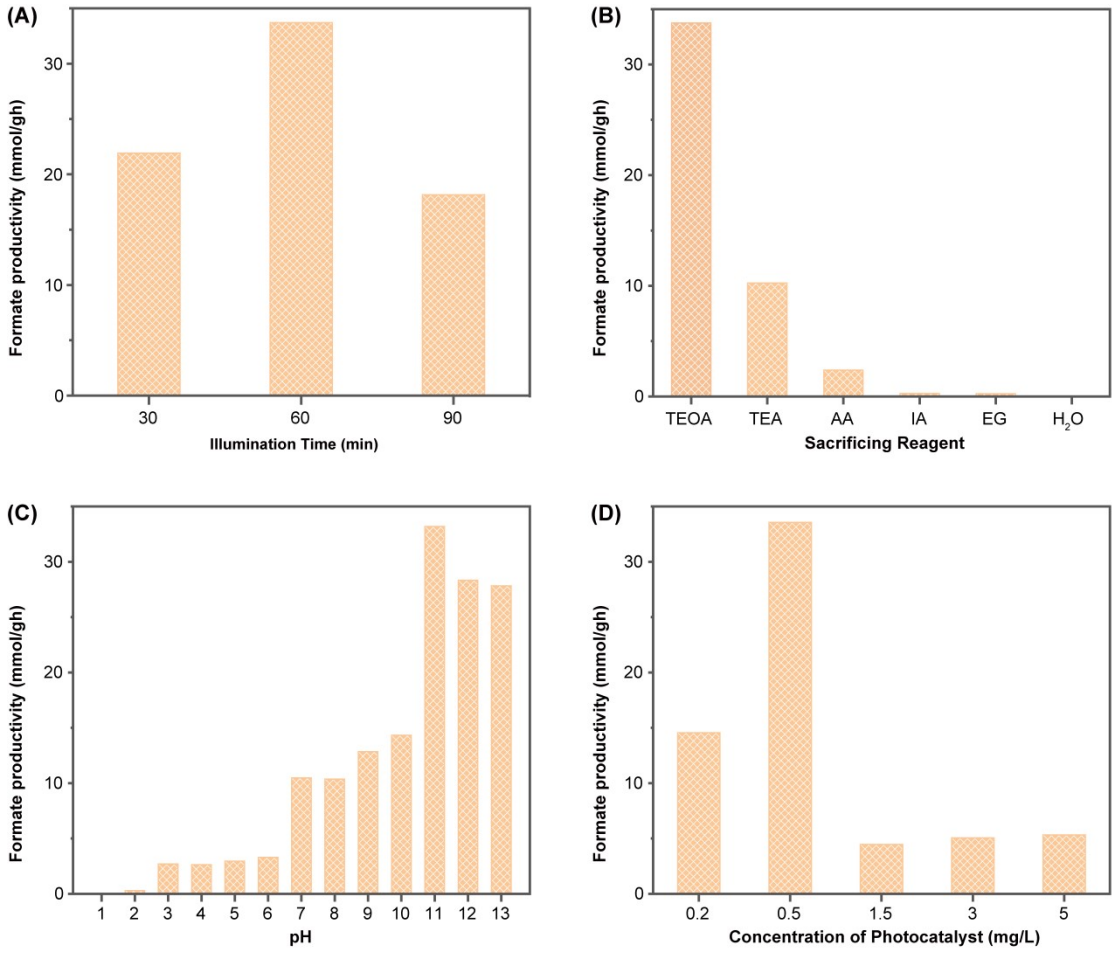

Fig. S20 Photocatalytic CO_2 conversion to formate (A) using BOC-L treated under different illumination time, (B) with different sacrificing reagent, (C) under different pH, and (D) with different catalyst mass, respectively.

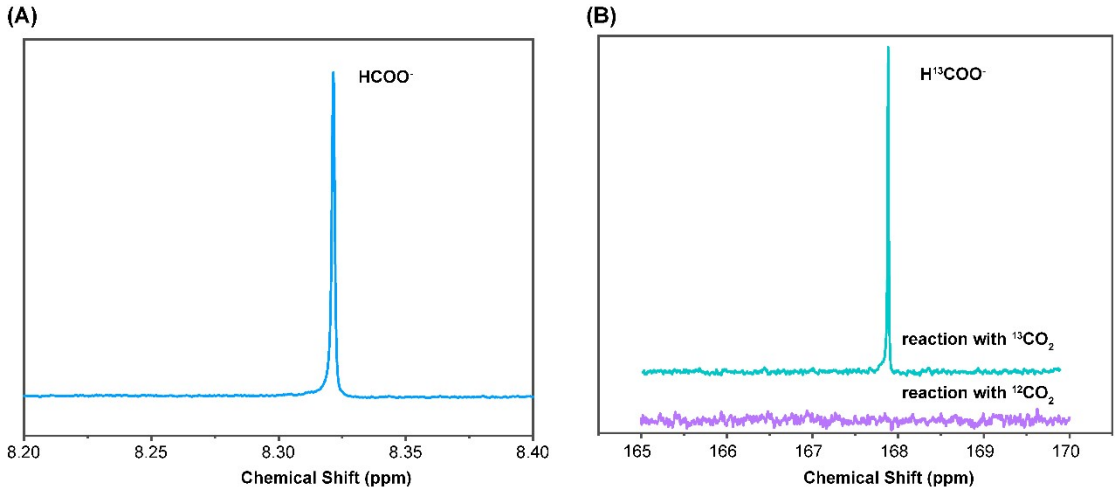

Fig. S21 (A) ^{1}H NMR and (B) ^{13}C NMR spectra of the solution after photocatalysis.

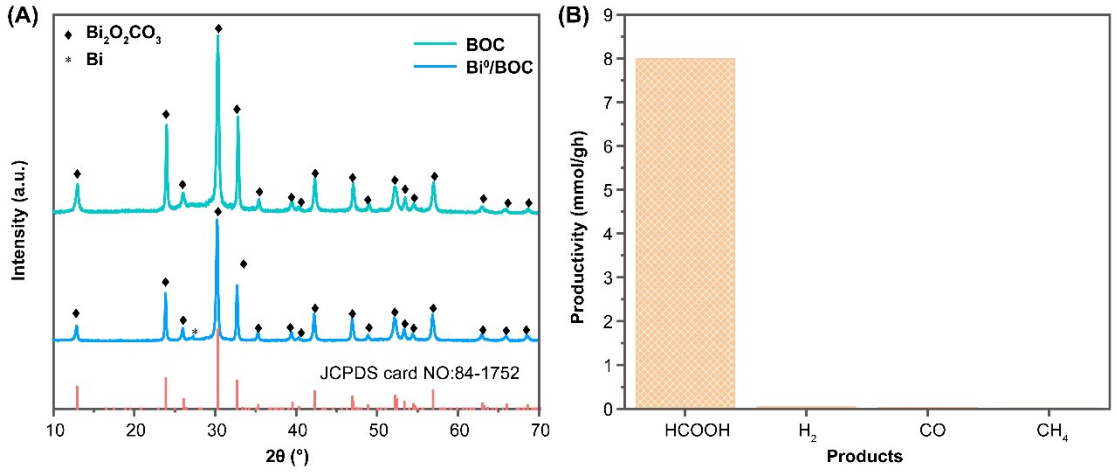

Fig. S22. (A) PXRD of BOC and Bi^{0}/BOC synthesized ex-situ. (B) Production rates of formate and other by-products of Bi^{0}/BOC.

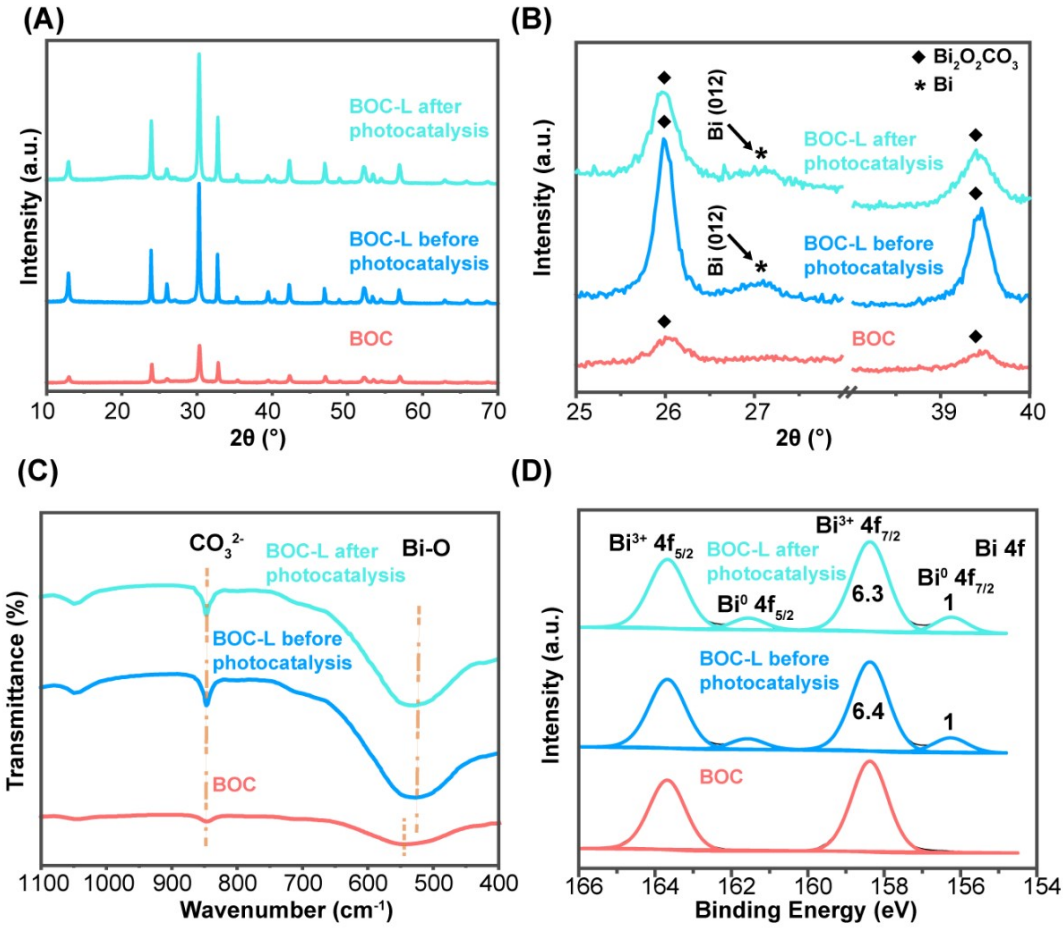

Fig. S23 (A) PXRD, (B) enlarged PXRD in the range of 25° to 40° of BOC, BOC-L before and after photocatalysis. (C) FT-IR, (D) XPS spectra of BOC, BOC-L before and after photocatalysis. The numbers in (D) shows the peak area ratio of Bi^{3+} to Bi^0.

Table S5. The FHWM of the highest intensity XRD diffraction peak corresponding to $Bi_2O_2CO_3$ and Bi^0 of BOC-L before and after photocatalysis.

Peaks in PXRD / Sample	(012) plane for Bi		(161) plane for $Bi_2O_2CO_3$	
	2θ (°)	FHWM (°)	2θ (°)	FHWM (°)
BOC-L before photocatalysis	27.1	0.68	30.3	0.26
BOC-L after photocatalysis	27.1	0.69	30.3	0.25

As illustrated in Fig. S22, the PXRD, FT-IR and XPS of BOC-L before and after photocatalytic CO_2 reduction have been compared. Little difference in the positions and the full height half width of the peaks corresponding to (161) plane of $Bi_2O_2CO_3$ and (012) plane of Bi^0 as summarized in Table S5, indicating that the crystallinity of both $Bi_2O_2CO_3$ and Bi^0 phases are varied little after photocatalysis. Consistently, the same blue shift of Bi-O stretching in comparing with BOC preserved after photocatalysis, implying the Bi vacancies are maintained. Moreover, two characteristic peaks located at 159.3 and 164.7 eV corresponding to Bi $4f_{7/2}$ and Bi $4f_{5/2}$ of Bi^{3+}, respectively, can be identified in the high-resolution Bi 4f XPS spectra of BOC-L before and after photocatalysis. In the meantime, peaks at 162.3 and 157 eV attributed to Bi^0 can be observed in BOC-L before and after photocatalysis (Fig. S22D). Additionally, the peak area ratio between Bi^{3+} and Bi^0 remains similar before and after photocatalysis (Figure S23D). All of the above results confirms that BOC-L maintains an unaltered structure and composition after photocatalytic CO_2 reduction.

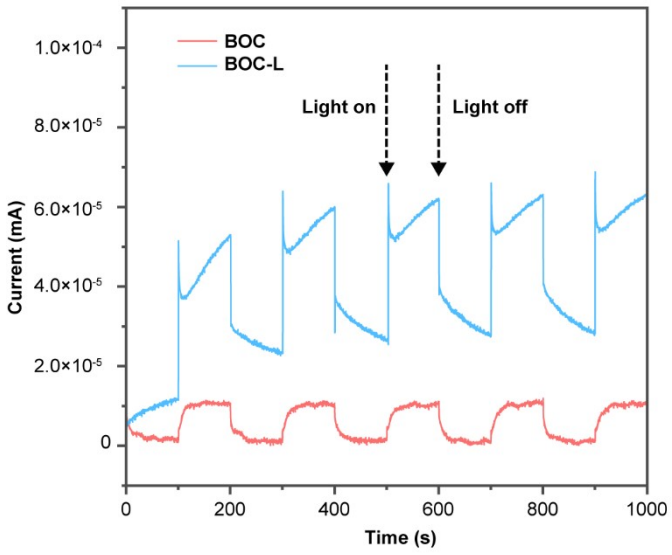

Fig. S24 Transient photocurrent curve of BOC and BOC-L.

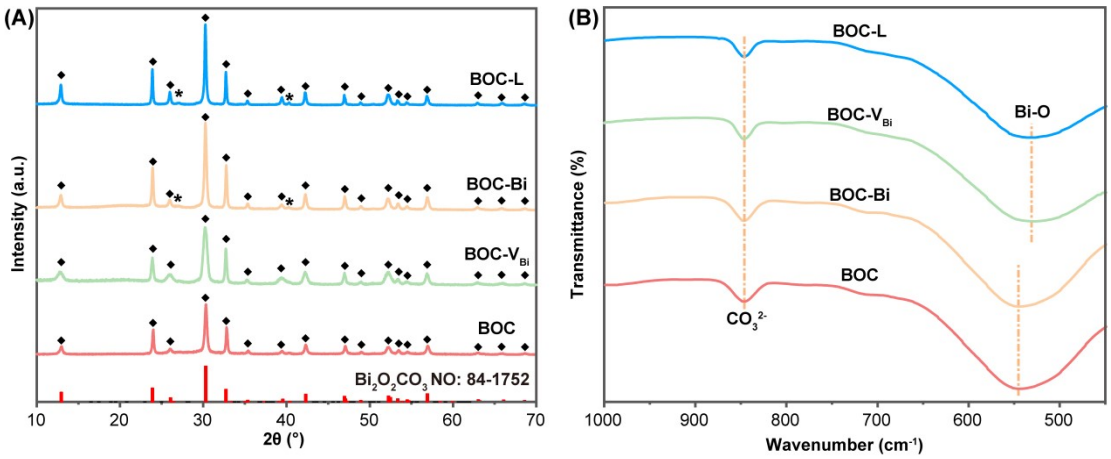

Fig. S25 (A) PXRD, (B) FT-IR spectra of BOC, BOC-L, BOC-Bi, and BOC-V_{Bi}.

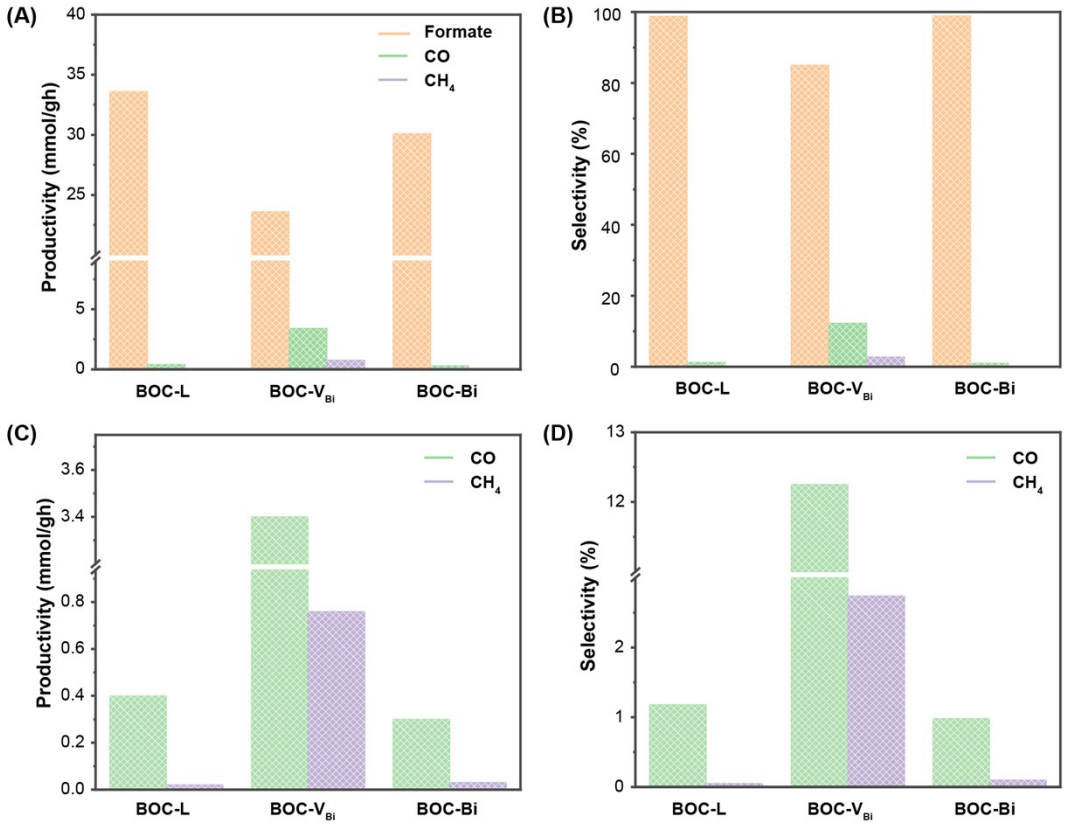

Fig. S26 The (A) and (B) productivity and selectivity of different products using BOC-L, BOC-Bi and BOC-V_{Bi}, respectively. (C) and (D) the enlarged charts show the productivity and selectivity of CO and CH_4 corresponding to (A) and (B), respectively.

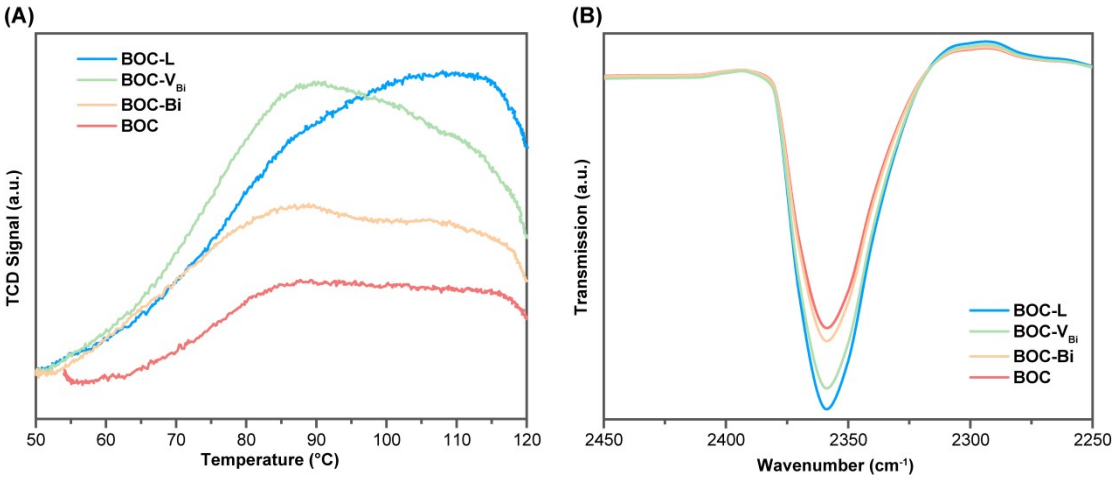

Fig. S27 (A) The TPD-CO_2 and (B) FT-IR of BOC, BOC-L, BOC-Bi, and BOC-V_{Bi}, respectively. As shown, BOC-L and BOC-V_{Bi} demonstrate comparable TCD signal, and FT-IR transmission intensity, which are higher than that of BOC and BOC-Bi. These results indicate that the presence of Bi vacancies is helpful to the adsorption of CO_2.

Reference:

1. P. Hohenberg and W. Kohn, *Physical Review*, 1964, **136**, B864-B871.
2. W. Kohn and L. J. Sham, *Physical Review*, 1965, **140**, A1133-A1138.
3. T. D. Kühne, M. Iannuzzi, M. Del Ben, V. V. Rybkin, P. Seewald, F. Stein, T. Laino, R. Z. Khaliullin, O. Schütt, F. Schiffmann, D. Golze, J. Wilhelm, S. Chulkov, M. H. Bani-Hashemian, V. Weber, U. Borštnik, M. Taillefumier, A. S. Jakobovits, A. Lazzaro, H. Pabst, T. Müller, R. Schade, M. Guidon, S. Andermatt, N. Holmberg, G. K. Schenter, A. Hehn, A. Bussy, F. Belleflamme, G. Tabacchi, A. Glöß, M. Lass, I. Bethune, C. J. Mundy, C. Plessl, M. Watkins, J. VandeVondele, M. Krack and J. Hutter, *The Journal of Chemical Physics*, 2020, **152**, 194103.
4. J. VandeVondele, M. Krack, F. Mohamed, M. Parrinello, T. Chassaing and J.

Hutter, *Computer Physics Communications*, 2005, **167**, 103-128.

5. J. P. Perdew, K. Burke and M. Ernzerhof, *Physical Review Letters*, 1996, **77**, 3865-3868.
6. J. VandeVondele and J. Hutter, *The Journal of Chemical Physics*, 2007, **127**, 114105.
7. S. Goedecker, M. Teter and J. Hutter, *Physical Review B*, 1996, **54**, 1703-1710.
8. M. Krack, *Theoretical Chemistry Accounts*, 2005, **114**, 145-152.
9. S. Grimme, J. Antony, S. Ehrlich and H. Krieg, *The Journal of Chemical Physics*, 2010, **132**, 154104.